Letter

Ferroelectricity in Epitaxial Perovskite Oxide Bi_2WO_6 Films with One-Unit-Cell Thickness

Song Zhou, Lei Liao, Lan Chen, Baojie Feng, Xiaoyue He, Xuedong Bai, Chuangye Song,* and Kehui Wu*

Cite This: https://doi.org/10.1021/acs.nanolett.3c01426

Read Online

ACCESS | ⊞ Metrics & More | ⊞ Article Recommendations | ⊞ Supporting Information
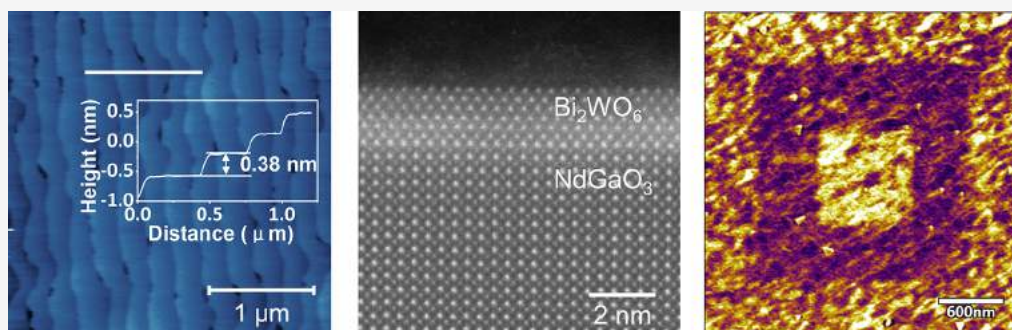
ABSTRACT: Retaining ferroelectricity in ultrathin films or nanostructures is crucial for miniaturizing ferroelectric devices, but it is a challenging task due to intrinsic depolarization and size effects. In this study, we have shown that it is possible to stably maintain in-plane polarization in an extremely thin, one-unit-cell thick epitaxial Bi_2WO_6 film. The use of a perfectly lattice-matched $NdGaO_3$ (110) substrate for the Bi_2WO_6 film minimizes strain and enhances stability. We attribute the residual polarization in this ultrathin film to the crystal stability of the Bi−O octahedral framework against structural distortions. Our findings suggest that ferroelectricity can surpass the critical thickness limit through proper strain engineering, and the Bi_2WO_6/$NdGaO_3$ (110) system presents a potential platform for designing low-energy consumption, nonvolatile ferroelectric memories.

KEYWORDS: perovskite oxide, ferroelectricity, pulsed laser deposition, piezoresponse force microscopy, scanning transmission electron microscopy

Ferroelectric materials, which exhibit spontaneous polarization due to their broken spatial-inversion symmetry, have a variety of fascinating applications such as piezoelectric sensors, nonvolatile data storage, and magnetoelectric devices.[1,2] The demand for miniaturizing electronic devices has increased the interest in low-energy-consumption ultrathin ferroelectric materials. In recent years, ferroelectricity has been observed in several ultrathin two-dimensional van der Waals materials, such as $CuInP_2S_6$,[3,4] In_2Se_3,[5] $MoTe_2$,[6] WTe_2,[7] SnS,[8] BA_2PbCl_4,[9] and twisted bilayer hBN.[10] However, the ferroelectricity in these 2D van der Waals systems is generally weaker than that of traditional ferroelectric ceramics.[11] Conventional strong ferroelectric materials are typically oxide films such as $PbZr_{0.2}Ti_{0.8}O_3$ and $BiFeO_3$. However, the complex surface reconstruction in these 3D oxides can result in the loss of long-range polarization ordering.[12] There have only been a few reports of ferroelectricity in ultrathin oxides with a few-unit-cell thickness, which were obtained through ion milling or water sacrificial exfoliation.[13,14] Realizing ferroelectricity on a large scale, ultrathin epitaxial oxide films remain a challenge and are highly desirable for electronic nanodevices.

The perovskite oxide Bi_2WO_6 (BWO) has a unique stacked arrangement of $[WO_4]^{2-}$ and $[Bi_2O_2]^{2+}$ layers, forming the structure known as the Aurivillius phase.[15] Furthermore, the in-plane polarization which parallels the film surface can effectively remove the limitation of the depolarization field, especially when the film thickness reduces. Currently, high-quality epitaxial BWO thin films can only be obtained when they are tens of nanometers thick and grown on $SrTiO_3$ or $LaAlO_3$ substrates.[16] Films that are less than 10 nm thick typically exhibit inhomogeneous island-growth modes,[17] limiting their use in electronic devices. Improving the epitaxial growth of ultrathin BWO films and understanding the ferroelectricity in these films are topics of high current interest.
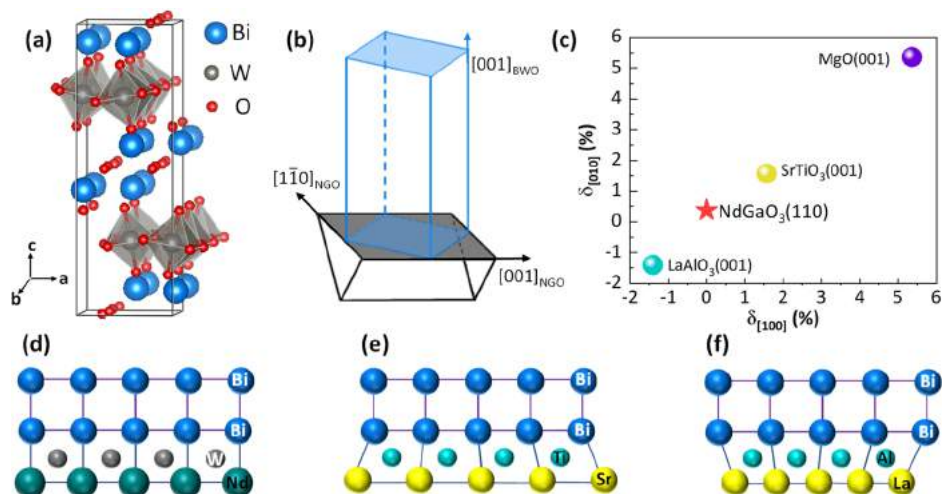
Figure 1. (a) Crystal structure of BWO. (b) Schematic of the cube-on-cube stacking of BWO on NGO (110) substrate. (c) Diagram of the lattice mismatch between BWO and commonly used substrates. (d−f) Illustration of the strain experienced by the substrate, (d) BWO on NGO (110), (e) BWO on $SrTiO_3$ (001), and (f) BWO on $LaAlO_3$ (001).
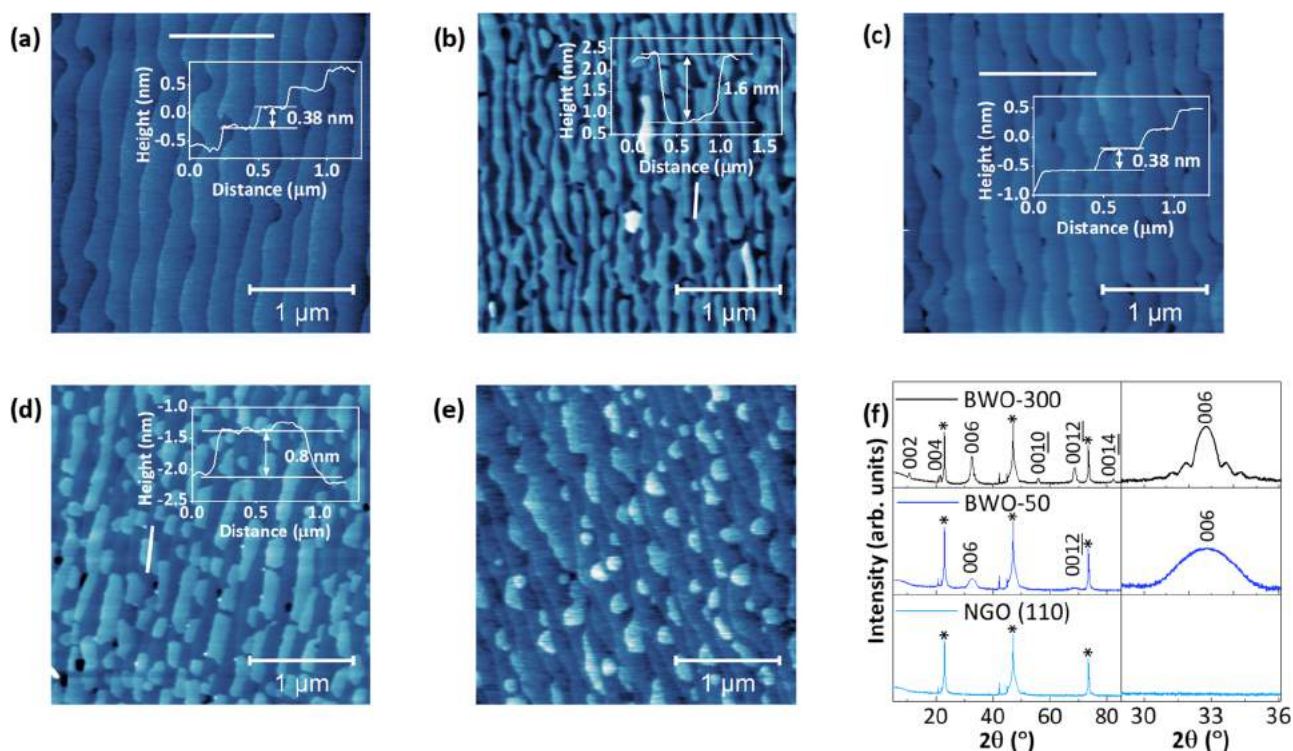
Figure 2. Illustration of the growth of BWO films on the NGO (110) substrate. (a) AFM topography of the chemically etched and annealed NGO (110) substrate, revealing an atomically flat surface. (b) BWO films after 50 laser pulses, where 1-UC-high islands can be seen on the NGO surface. (c) BWO films after 80 laser pulses, which show complete coverage of the NGO surface and a morphology that perfectly follows the substrate, as seen in the height profile insets. (d) BWO films after 100 laser pulses. The insets in (a)−(d) show the height profile along the white solid lines. (e) BWO films after 300 laser pulses. (f) XRD patterns of the NGO (110) substrate, BWO films with 50 laser pulses (BWO-50), and 300 laser pulses (BWO-300) are also presented. The zoomed-in (006) XRD pattern can be found in the right panel.

In this study, we present the successful growth of extremely thin, high-quality epitaxial BWO films with a thickness as low as one unit cell (UC) on a (110)-oriented $NdGaO_3$ (NGO) substrate using pulsed laser deposition (PLD). Atomic force microscopy (AFM) reveals layer-by-layer growth down to the 1-UC limit, and the perfect crystalline nature of the BWO film is further confirmed by aberration-corrected scanning transmission electron microscopy (STEM) images and X-ray diffraction (XRD). Moreover, in-plane ferroelectric domains

with multiple preferred orientations are clearly seen through piezoresponse force microscopy (PFM), which can be switched with a 5 V bias voltage applied between the tip and sample. The epitaxial ultrathin BWO films surpass the critical thickness limit of ferroelectricity in perovskite oxides and hold promise for future nanodevice applications.

Figure 1a illustrates that the (001)-oriented BWO has a layered perovskite structure characterized by alternating $[WO_4]^{2-}$ and $[Bi_2O_2]^{2+}$ layers. On the other hand, the NGO
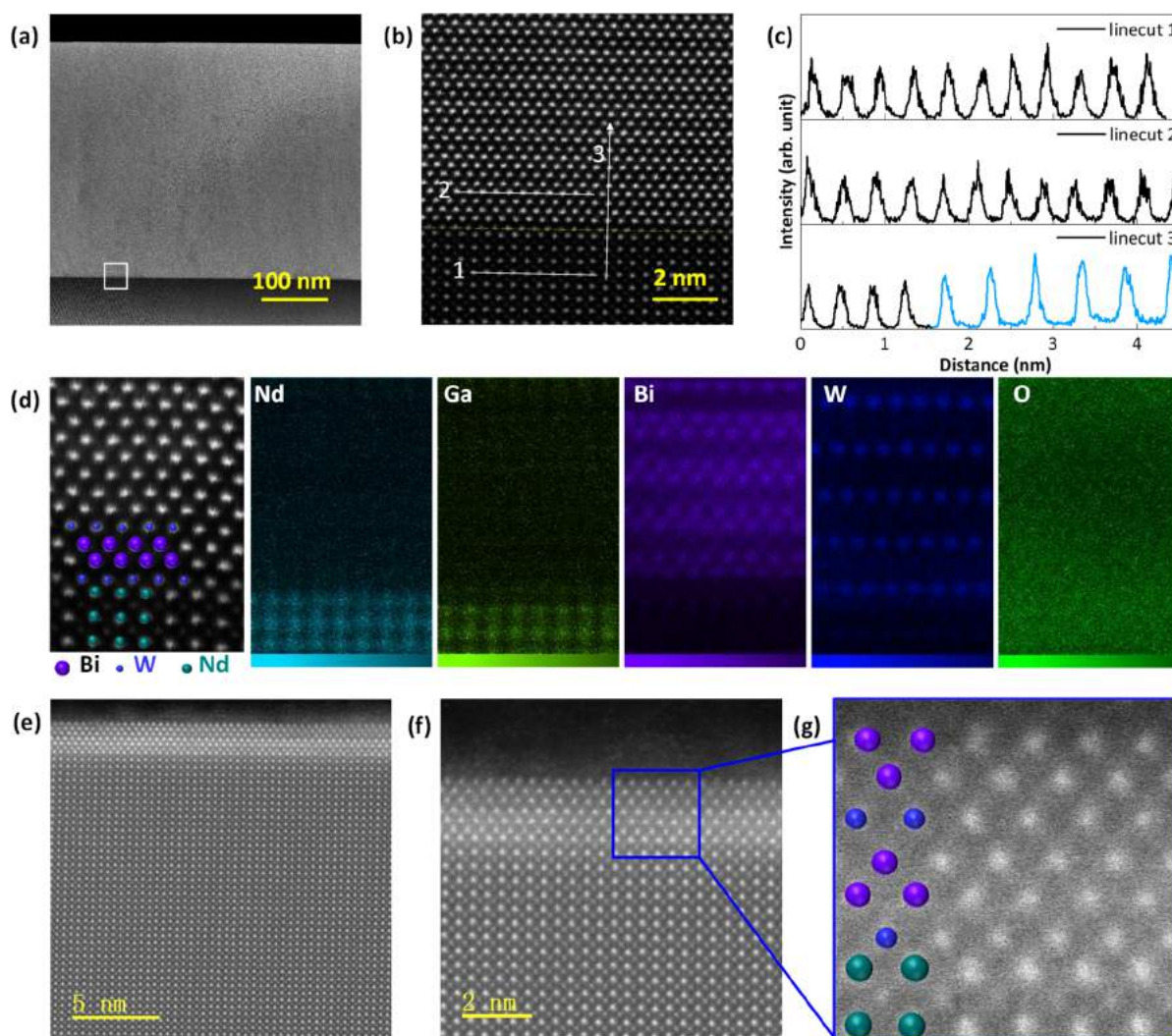
Figure 3. Crystallographic structure of the BWO/NGO interface. (a) A low-magnification cross-sectional STEM image of a 350 nm BWO/NGO (110) film. (b) The zoom-in image of the square solid area in (a), revealing an atomically resolved STEM image with a clearly defined BWO/NGO interface as marked by the yellow dashed line. (c) Line profiles along the white solid lines in (b): line 1 along the NdO layer, line 2 along the BiO layer, and line 3 across the BWO/NGO interface. (d) Representative high-angle annular dark-field STEM image and energy-dispersive spectroscopy (EDS) maps of the BWO/NGO (110) interface. (e) High-resolution STEM image along the BWO [110] zone axis. (f) Zoom-in image of the 1-UC BWO film grown on the NGO (110) substrate. (g) The magnified STEM image of the blue square part in (f).

has an orthorhombic crystal structure with lattice parameters a = 0.5428 nm, b = 0.5498 nm, and c = 0.7708 nm.[18,19] The corresponding in-plane lattice constants of the NGO (110) surface are $a_{[1\bar{1}0]} = \sqrt{(a^2 + b^2)}$ = 0.773 nm and $a_{[001]} = c$ = 0.7708 nm. The epitaxial relationship between the BWO films and the NGO (110) surface is depicted in Figure 1b, which shows a "cube-on-cube" relationship with the BWO (001) cube rotated in-plane by 45° relative to the $[110]_{NGO}$ direction. The lattice constant of the pseudocube in the NGO (110) surface is $a_{NGO} = \frac{1}{2}\sqrt{a_{[1\bar{1}0]}^2 + a_{[001]}^2}$ = 0.5458 nm, and the in-plane lattice mismatch between the NGO and BWO is defined as $\delta = (a_{NGO} - a_{BWO})/a_{BWO}$, with a_{BWO} being the ortho-rhombic BWO lattice constants $a_{[100]}$ = 0.5437 nm, $a_{[110]}$ = 0.5458 nm, and $a_{[100]}$ = 1.6430 nm. This results in a small δ = 0.38% at the BWO/NGO (110) interface compared to the widely used $SrTiO_3$(001) substrate, which leads to a lattice mismatch of 1.57% at the BWO/$SrTiO_3$ (001) interface. Figure 1c compares the lattice mismatch of BWO on different

commonly used substrates, indicating the large lattice mismatches on $LaAlO_3$ (δ = −1.4%) and MgO (δ = 5.36%). The large lattice mismatch in BWO/$SrTiO_3$ (Figure 1e) and BWO/$LaAlO_3$ (Figure 1f) can result in significant tensile and compressive strains at the interface, leading to the formation of discontinuous morphologies in thinner films (below 30 nm, or about 20 UC in thickness) with flat islands and hollows between islands, as shown in Figures S1 and S2 of the Supporting Information. In contrast, the relatively small lattice mismatch in BWO/NGO(110) offers an ideal strain-free platform for the epitaxial growth of high-quality ultrathin BWO films.

Prior to the growth of the BWO films, the NGO (110) substrate was subjected to chemical treatment to attain atomically flat surfaces. As seen in Figure 2a, this treatment resulted in an atomically flat surface, with a step height of ~0.38 nm, which matches well with the combination of one NdO and one GaO_2 atomic layer. The surface is believed to be terminated by the NdO layer, as reported previously,[18,20] and this will be further confirmed by our STEM images later in the
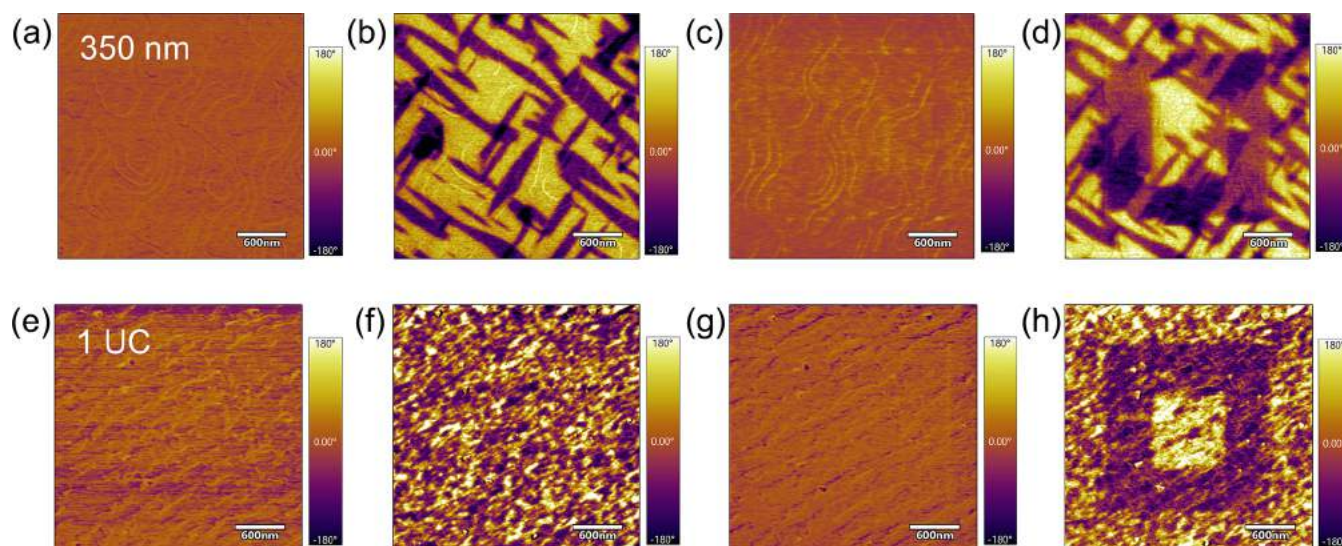
Figure 4. Ferroelectric characterization and polarization switching. Vertical (a) and lateral (b) PFM images of the 350-nm-thick BWO film, respectively. Vertical (c) and lateral (d) PFM images after applying a voltage of 18 and −18 V to the AFM tip via the litho-PFM mode, where the in-plane ferroelectric domains have been switched and the out-of-plane polarization remains unchanged. Vertical (e) and lateral (f) PFM images of the 1-UC BWO film. Vertical (g) and lateral (h) PFM images after applying a voltage of 5 and −5 V to the AFM tip via the litho-PFM mode.

text. BWO films were deposited on the treated NGO (110) substrate through PLD (see the Methods section in the Supporting Information for more details).

It is fascinating that we can precisely control the film thickness down to a single unit cell (UC) by varying the number of pulses during deposition. Figures 2b−e show the gradual increase in pulse counts from 50 to 80, 100, and finally 300, revealing the evolution of surface morphology. In Figure 2b, flat BWO islands cover over half of the NGO (110) surface with a uniform height of approximately 1.6 nm, which corresponds to a single UC of BWO along the [001] direction. The coverage is calculated to be 60% through image processing software. As the pulse counts increase, these 1-UC BWO islands grow epitaxially along the step edges of the NGO (110) substrate. Upon reaching 80 pulse counts, the 1-UC BWO film fully covered the NGO surface, mimicking its morphology (as seen in Figure 2c). The inset image displays a step height of 0.38 nm, which is identical with the NGO (110) substrate. Hence, an almost ideal 1-UC BWO film is formed. When the deposition pulse increases to 100 counts, second layer BWO islands will form on top of the completed first monolayer, as shown in Figure 2d. The height of the BWO islands is found to be 0.82 nm, which aligns with the half-unit-cell height of BWO.[16] An estimated coverage of ~45% for the half-unit-cell BWO islands is determined. The deposition flux of BWO in this situation can be calculated as 0.02 nm/pulse, which is in perfect agreement with the values obtained from both Figures 2b and 2c. This consistency supports the designation of the first- and second-layer films as 1- and 1.5-UC BWO films, respectively. The successful layer-by-layer epitaxial growth of BWO films on the NGO (110) substrate with a minimum film thickness of 1 UC is achieved. The good morphology of films can be maintained even when increasing the pulse counts to 300 (as seen in Figure 2e).

To further verify the crystalline quality of the as-grown BWO films, we conducted the XRD measurements. Figure 2f presents the XRD patterns of the BWO films with 300 (black) and 50 (blue) pulse counts with the XRD pattern of the NGO (110) substrate (cyan) included for comparison. It should be

noted that the peak around 42° comes from the Cu K_β line of the NGO (110) substrate. Along with the set of (110) diffraction peaks from the NGO substrate (marked with asterisks), another set of (001) oriented diffraction peaks can be easily identified and are assumed to belong to the BWO films. The BWO film with 50 pulse counts is so thin that its XRD diffraction intensity is relatively low, and only the (006) and (0012) peaks are visible. Notably, as seen in the right panel of Figure 2f, prominent Pendellösung fringes appear in the BWO (006) peak when the pulse counts are increased from 50 to 300, which strongly indicates the smooth film surface and high-quality epitaxy of the BWO films on the NGO substrate. The (006) diffraction peak of the BWO films is centered at $2\theta = 32.725°$. Based on $n\lambda = 2d \sin \theta$, the lattice parameter along the [001] direction can then be calculated as $c = 1.642$ nm, which aligns perfectly with the theoretical value and demonstrates a nearly strain-free epitaxial growth. In addition to the principal reflections in XRD, we have performed in-plane XRD (i.e., phi scans) of the 80-pulse-count BWO film along the (113) orientation. As is expected of orthorhombic crystals, the phi scan of the BWO (113) reflection exhibits four diffraction peaks through 360° of rotation (see Figure S3), which further confirms the epitaxial growth of the high-quality BWO film.

To further understand the atomic structure of the BWO/NGO(110) films, an aberration-corrected STEM measurement has been performed on both a 350-nm-thick BWO film and a 1UC-thick film. The results of the measurements are shown in Figure 3. Figure 3a displays a high-angle annular dark-field (HAADF) image of the cross section of the 350 nm BWO/NGO film, which provides a large-area overview. The yellow dashed line in the zoomed-in image (Figure 3b) shows a well-defined, atomically sharp interface. On the NGO substrate side, bright spots correspond to the Nd atoms, indicating that the surface of the NGO substrate is NdO-terminated, as previously assumed. On the BWO film side, the $[WO_4]^{2-}$ layer is first formed on the NdO-terminated NGO substrate, followed by the $[Bi_2O_2]^{2+}$ layer. The line profiles in Figure 3c reveal that the lattice spacing between the neighboring NdO

layers is c = 0.385 nm, and the in-plane and out-of-plane spacings of the BWO layers are 0.386 and 0.274 nm ($c/6$), respectively. Both the XRD patterns and STEM images confirm that the BWO/NGO(110) interface is nearly strain-free. The energy-dispersive X-ray spectroscopy (EDS) chemical maps at the interface, shown in Figure 3d, indicate that there is no chemical intermixing at the atomically sharp interface. The high-quality BWO/NGO(110) interface demonstrates that the strain clamping from the substrate is negligible in the BWO/NGO(110) heterostructure due to the relatively small lattice misfit between the film and substrate. In addition, we also performed the STEM measurement on the 1 UC BWO film to investigate its epitaxy and crystallinity. As shown in Figure 3e, bright spots correspond to the Nd atoms on the NGO substrate side, indicating that the surface of the NGO substrate is NdO-terminated, which is consistent with the STEM measurement of the 350-nm-thick BWO film in Figure 3a. On the BWO film side, the $[WO_4]^{2-}$ layer is first formed on the NdO-terminated NGO substrate, followed by the $[Bi_2O_2]^{2+}-[WO_4]^{2-}-[Bi_2O_2]^{2+}$ sandwiched structure, indicating the formation of the high-quality 1-UC BWO crystal on the NGO substrate.

The setup for the PFM experiment is depicted in Figure S4, which is similar to the previous work.[16] Although BWO thin films have been reported to possess ferroelectricity when the film thickness is in the tens of nanometers range,[16] we examined the ferroelectricity of BWO films of various thicknesses, down to a single-unit-cell limit. Figure 4 displays the ferroelectric domains and polarization switching observed through vector-PFM and Litho-PFM modes. In Figures 4a,b, we show the vertical and lateral ferroelectric polarization of a 350-nm-thick BWO film collected simultaneously through vector PFM mode. It is evident that the polarization field in this bulklike film primarily lies in the in-plane direction without any out-of-plane projection. The typical four-color domains are also clearly visible, indicating four preferential ferroelectric polarization configurations, which is consistent with previous report.[16] To perform polarization switching, we applied 18 and −18 V voltage to the AFM tip through litho-PFM mode and scanned the tip across a predefined area. After tip writing, the ferroelectric domains were switched in the writing area, as seen in Figure 4d. Although the electric field applied for writing was primarily in a perpendicular direction, the predominant effect on polarization switching was in the in-plane direction due to the in-plane component of the electric field under the tip, and the remaining perpendicular polarization was negligible (Figure 4c).

The potential presence of ferroelectricity in a 1-UC BWO film is particularly intriguing. Using the same approach, we measured the ferroelectric properties of the 1-UC BWO film using PFM, as shown in Figure 4f. The in-plane polarization still dominates the 1-UC BWO film, as seen from the in-plane PFM image, while the out-of-plane polarization is minimal, as seen from the smooth out-of-plane PFM image (Figure 4e). It is notable that unlike the large (approximately hundreds of nanometers) polarization domains observed in the 350-nm-thick film (Figure 4b), the in-plane polarization domains in the 1-UC-thick film appear rather small (typically a few tens of nanometers), close to the spatial resolution of PFM. The color histogram in Figure S6 shows multiple peaks roughly corresponding to the four polarization orientations, but we cannot exclude the existence of additional polarization orientations due to the limited resolution of PFM. In addition,

the PFM amplitude channel, shown in Figure S7, confirms the simultaneous presence of ferroelectric response in the 1-UC BWO film. It is notable that in the above switching experiments, the applied electric field is primarily in the direction perpendicular to the surface, while the polarization in BWO films is mostly in-plne. In such a configuration we were not able to obtain a characteristic P-E loop curve of ferroelectric switching. In order to overcome this difficulty, as shown in Figure S5a, we fabricated a gold electrode on a part of this 1-UC BWO film, and an AFM tip was brought close to the edge of the electrode to apply the electric voltage. Thus, an in-plane electric field was generated between the tip and gold electrode. A characteristic P-E loop curve was then obtained as shown in Figure S5b. The phase difference between the two polarization states is 180°, and the minima in the amplitude loop coincide with the switching voltages in the phase signal, indicating the ferroelectric nature. Moreover, in order to study the ferroelectric retention behavior, the in-plane PFM phase and amplitude images of the switched domains are shown in Figures S8a and S8b. Interestingly, there is no obvious change in the written domains after 24 h (see Figures S8c and S8d). The ferroelectric retention behavior of the 1-UC BWO film evidences the robust stability of the ferroelectric polarization against the complex perturbations. To the best of our knowledge, perovskite oxide films have not exhibited ferroelectricity in such a two-dimensional limit before. More importantly, the same writing process applied to a predefined square-shaped area of the 1 UC film with a voltage of 5 and −5 V, resulting in clear polarization switching; i.e., the polarization switching occurs in the in-plane direction (Figure 4h), with no significant impact on the c-axis polarization (Figure 4g).

As to the origin of the ferroelectricity in the BWO crystal, the theoretical value of the ferroelectric displacement of W cations from the center of oxygen octahedral is around 30−40 pm,[15,21] while the recent experiment reveals the average atomic displacement of W cations to be around 20 pm,[22] which is definitely smaller than the theoretical value. It implies that W atomic displacement may not be the only origin of the ferroelectric polarization in the BWO crystal, and there may be other contribution to the in-plane ferroelectric polarization in the BWO, e.g., the displacement of Bi atoms relative to their octahedrons in the $[Bi_2O_2]^{2-}$ fluorite-like layer in the BWO crystal;[16,23,24] it still remains a pending issue and deserves more detailed investigations. Although the BWO suffers negligible strain clamping from the substrate when grown on the NGO (110) crystal, the surface-to-volume ratio of oxygen dangling bond can dramatically increase if we make the BWO film ultrathin (e.g., monolayer). Given that the dangling bonds can act as the chemical active sites for the surface adsorption,[25] the complicated surface structures further bring big challenges for the crystal stability at this ultrathin limit, for example, the octahedra rotation, lattice reconstruction, atomic defects, and so on. Fortunately, the high-quality epitaxy maintains the intrinsic orthorhombic crystal structure and in-plane ferroelectric polarization in the 1-UC BWO/NGO (110) case. It implies that the strong stability of the Bi−O octahedra framework can stand against the adverse factors at the surface and prevent complicated lattice reconstructions, which could otherwise disrupt the stable in-plane spontaneous polarization.

To conclude, we have found a perfect substrate, NGO (110), for growing high-quality BWO films, even down to a thickness of 1 UC. The quality of these ultrathin BWO films is superior to any previous attempts on other substrates because

of the ideal lattice matching between NGO (110) and BWO (001). Our results show that even down to one unit cell, BWO retains its ferroelectricity. As a perovskite oxide, BWO has a strong polarization field, and the significantly smaller ferro-electric domain size in the 1-UC film offers potential advantages for addressing the scaling challenges in the modern electronics industry.

■ ASSOCIATED CONTENT

ⓈⒾ Supporting Information

The Supporting Information is available free of charge at https://pubs.acs.org/doi/10.1021/acs.nanolett.3c01426.

> Details of the experimental methods for sample preparation, PFM characterizations, surface topography, and X-ray diffraction phi scans in Figures S1−S8 (PDF)

■ AUTHOR INFORMATION

Corresponding Authors

Chuangye Song − *Institute of Physics, Chinese Academy of Sciences, Beijing 100190, China; Songshan Lake Materials Laboratory, Dongguan, Guangdong 523808, China;* Ⓞ orcid.org/0000-0002-3152-1576; Email: cyesong@iphy.ac.cn

Kehui Wu − *Institute of Physics, Chinese Academy of Sciences, Beijing 100190, China; School of Physical Sciences, University of Chinese Academy of Sciences, Beijing 100049, China; Songshan Lake Materials Laboratory, Dongguan, Guangdong 523808, China; Interdisciplinary Institute of Light-Element Quantum Materials and Research Center for Light-Element Advanced Materials, Peking University, Beijing 100871, China;* Ⓞ orcid.org/0000-0002-7698-5673; Email: khwu@iphy.ac.cn

Authors

Song Zhou − *Institute of Physics, Chinese Academy of Sciences, Beijing 100190, China; School of Physical Sciences, University of Chinese Academy of Sciences, Beijing 100049, China*

Lei Liao − *Institute of Physics, Chinese Academy of Sciences, Beijing 100190, China; School of Physical Sciences, University of Chinese Academy of Sciences, Beijing 100049, China*

Lan Chen − *Institute of Physics, Chinese Academy of Sciences, Beijing 100190, China; School of Physical Sciences, University of Chinese Academy of Sciences, Beijing 100049, China;* Ⓞ orcid.org/0000-0003-4426-9944

Baojie Feng − *Institute of Physics, Chinese Academy of Sciences, Beijing 100190, China; School of Physical Sciences, University of Chinese Academy of Sciences, Beijing 100049, China;* Ⓞ orcid.org/0000-0003-2332-7949

Xiaoyue He − *Songshan Lake Materials Laboratory, Dongguan, Guangdong 523808, China*

Xuedong Bai − *Institute of Physics, Chinese Academy of Sciences, Beijing 100190, China; School of Physical Sciences, University of Chinese Academy of Sciences, Beijing 100049, China;* Ⓞ orcid.org/0000-0002-1403-491X

Complete contact information is available at:
https://pubs.acs.org/10.1021/acs.nanolett.3c01426

Author Contributions

K.W. and S.C. conceived the research. Z.S. prepared the samples and performed AFM, PFM, and XRD experiments; L.L. and Z.S. performed TEM experiments; all authors contributed to the discussion of the data and writing of the manuscript.

Notes

The authors declare no competing financial interest.

■ REFERENCES

(1) Hu, Z.; Tian, M.; Nysten, B.; Jonas, A. M. Regular arrays of highly ordered ferroelectric polymer nanostructures for non-volatile low-voltage memories. *Nat. Mater.* **2009**, *8*, 62−67.

(2) Spaldin, N. A.; Ramesh, R. Advances in magnetoelectric multiferroics. *Nat. Mater.* **2019**, *18*, 203−212.

(3) Deng, J.; Liu, Y.; Li, M.; Xu, S.; Lun, Y.; Lv, P.; Xia, T.; Gao, P.; Wang, X.; Hong, J. Thickness-dependent in-plane polarization and structural phase transition in van der Waals ferroelectric $CuInP_2S_6$. *Small* **2020**, *16*, 1904529.

(4) Jiang, X.; Wang, X.; Wang, X.; Zhang, X.; Niu, R.; Deng, J.; Xu, S.; Lun, Y.; Liu, Y.; Xia, T.; Lu, J.; Hong, J. Manipulation of current rectification in van der Waals ferroionic $CuInP_2S_6$. *Nat. Commun.* **2022**, *13*, 574.

(5) Zheng, C.; Yu, L.; Zhu, L.; Collins, J. L.; Kim, D.; Lou, Y.; Xu, C.; Li, M.; Wei, Z.; Zhang, Y.; Edmonds, M. T.; Li, S.; Seidel, J.; Zhu, Y.; Liu, J. Z.; Tang, W.-X.; Fuhrer, M. S. Room temperature in-plane ferroelectricity in van der Waals In_2Se_3. *Sci. Adv.* **2018**, *4*, No. eaar7720.

(6) Yuan, S.; Luo, X.; Chan, H. L.; Xiao, C.; Dai, Y.; Xie, M.; Hao, J. Room-temperature ferroelectricity in $MoTe_2$ down to the atomic monolayer limit. *Nat. Commun.* **2019**, *10*, 1775.

(7) Fei, Z.; Zhao, W.; Palomaki, T. A.; Sun, B.; Miller, M. K.; Zhao, Z.; Yan, J.; Xu, X.; Cobden, D. H. Ferroelectric switching of a two-dimensional metal. *Nature* **2018**, *560*, 336−339.

(8) Higashitarumizu, N.; Kawamoto, H.; Lee, C.-J.; Lin, B.-H.; Chu, F.-H.; Yonemori, I.; Nishimura, T.; Wakabayashi, K.; Chang, W.-H.; Nagashio, K. Purely in-plane ferroelectricity in monolayer SnS at room temperature. *Nat. Commun.* **2020**, *11*, 2428.

(9) You, L.; Liu, F.; Li, H.; Hu, Y.; Zhou, S.; Chang, L.; Zhou, Y.; Fu, Q.; Yuan, G.; Dong, S.; Fan, H. J.; Gruverman, A.; Liu, Z.; Wang, J. In-plane ferroelectricity in thin flakes of van der Waals hybrid perovskite. *Adv. Mater.* **2018**, *30*, 1803249.

(10) Yasuda, K.; Wang, X.; Watanabe, K.; Taniguchi, T.; Jarillo-Herrero, P. Stacking-engineered ferroelectricity in bilayer boron nitride. *Science* **2021**, *372*, 1458−1462.

(11) You, L.; Zhang, Y.; Zhou, S.; Chaturvedi, A.; Morris, S. A.; Liu, F.; Chang, L.; Ichinose, D.; Funakubo, H.; Hu, W.; et al. Origin of giant negative piezoelectricity in a layered van der Waals ferroelectric. *Sci. Adv.* **2019**, *5*, No. eaav3780.

(12) Gao, P.; Liu, H.-J.; Huang, Y.-L.; Chu, Y.-H.; Ishikawa, R.; Feng, B.; Jiang, Y.; Shibata, N.; Wang, E.-G.; Ikuhara, Y. Atomic mechanism of polarization-controlled surface reconstruction in ferroelectric thin films. *Nat. Commun.* **2016**, *7*, 11318.

(13) Ji, D.; Cai, S.; Paudel, T. R.; Sun, H.; Zhang, C.; Han, L.; Wei, Y.; Zang, Y.; Gu, M.; Zhang, Y.; Gao, W.; Huyan, H.; Guo, W.; Wu, D.; Gu, Z.; Tsymbal, E. Y.; Wang, P.; Nie, Y.; Pan, X. Freestanding crystalline oxide perovskites down to the monolayer limit. *Nature* **2019**, *570*, 87−90.

(14) Gao, P.; Zhang, Z.; Li, M.; Ishikawa, R.; Feng, B.; Liu, H.-J.; Huang, Y.-L.; Shibata, N.; Ma, X.; Chen, S.; Zhang, J.; Liu, K.; Wang, E.-G.; Yu, D.; Liao, L.; Chu, Y.-H.; Ikuhara, Y. Possible absence of

critical thickness and size effect in ultrathin perovskite ferroelectric films. *Nat. Commun.* **2017**, *8*, 15549.

(15) Wolfe, R. W.; Newnahm, R. E.; Kay, M. I. Crystal structure of Bi$_2$WO$_6$. *Solid State Commun.* **1969**, *7*, 1797−1801.

(16) Wang, C.; Ke, X.; Wang, J.; Liang, R.; Luo, Z.; Tian, Y.; Yi, D.; Zhang, Q.; Wang, J.; Han, X. F.; Van Tendeloo, G.; Chen, L. Q.; Nan, C. W.; Ramesh, R.; Zhang, J. Ferroelastic switching in a layered-perovskite thin film. *Nat. Commun.* **2016**, *7*, 10636.

(17) Song, C.; Gao, J.; Liu, J.; Yang, Y.; Tian, C.; Hong, J.; Weng, H.; Zhang, J. Atomically resolved edge states on a layered ferroelectric oxide. *ACS Appl. Mater. Interfaces* **2020**, *12*, 4150−4154.

(18) Ohnishi, T.; Takahashi, K.; Nakamura, M.; Kawasaki, M.; Yoshimoto, M.; Koinuma, H. A-site layer terminated perovskite substrate: NdGaO$_3$. *Appl. Phys. Lett.* **1999**, *74*, 2531−2533.

(19) Boschker, H.; Mathews, M.; Houwman, E. P.; Nishikawa, H.; Vailionis, A.; Koster, G.; Rijnders, G.; Blank, D. H. A. Strong uniaxial in-plane magnetic anisotropy of (001)-and (011)-oriented La$_{0.67}$Sr$_{0.33}$MnO$_3$ thin films on NdGaO$_3$ substrates. *Phys. Rev. B* **2009**, *79*, 214425.

(20) Cavallaro, A.; Harrington, G. F.; Skinner, S. J.; Kilner, J. A. Controlling the surface termination of NdGaO$_3$ (110): the role of the gas atmosphere. *Nanoscale* **2014**, *6*, 7263−7273.

(21) Okudera, H.; Sakai, Y.; Yamagata, K.; Takeda, H. Structure of russellite (Bi$_2$WO$_6$): origin of ferroelectricity and the effect of the stereoactive lone electron pair on the structure. *Acta Crystallogr. B* **2018**, *74*, 295−303.

(22) Jeong, J.; Mun, J.; Das, S.; Kim, J.; Kim, J. R.; Peng, W.; Kim, M.; Noh, T. W. Growth and atomically resolved polarization mapping of ferroelectric Bi$_2$WO$_6$ thin films. *ACS Appl. Electron. Mater.* **2021**, *3*, 1023−1030.

(23) Machado, R.; Stachiotti, M. G.; Migoni, R. L.; Tera, A. H. First-principles determination of ferroelectric instabilities in Aurivillius compounds. *Phys. Rev. B* **2004**, *70*, 214112.

(24) Withers, R. L.; Thompson, J. G.; Rae, A. D. The crystal chemistry underlying ferroelectricity in Bi$_4$Ti$_3$O$_{12}$, Bi$_3$TiNbO$_9$, and Bi$_2$WO$_6$. *J. Solid State Chem.* **1991**, *94*, 404−417.

(25) Zhou, Y.; Zhang, Y.; Lin, M.; Long, J.; Zhang, Z.; Lin, H.; Wu, J. C.; Wang, X. Monolayered Bi$_2$WO$_6$ nanosheets mimicking heterojunction interface with open surfaces for photocatalysis. *Nat. Commun.* **2015**, *6*, 8340.